STM JOURNALS

Journal of
Experimental & Applied Mechanics

https://journals.stmjournals.com/joeam

ISSN: 2230-9845 (Online)
ISSN: 2321-516X (Print)
Volume 17, Issue 2, 2026
May–August
DOI (Journal): 10.37591/JoEAM

Research JoEAM

Experimental Study on Microstructural Evolution and Tensile Properties of Robotic Pulse MIG Welded Steel

Vivekanand[1,*] and Raja Somadder[2]

Abstract

Robotic pulse Metal Inert Gas (MIG) welding has emerged as an advanced joining technique capable of producing superior weld quality through precise control of welding parameters. The present study evaluates the influence of welding parameters on the microstructural evolution and tensile properties of steel weldments fabricated using robotic pulse MIG welding and compares the results with conventional pulse MIG welding. Microstructural characterization was carried out using Scanning Electron Microscopy (SEM) and Energy Dispersive X-ray Spectroscopy (EDS), while tensile properties were determined using a Universal Testing Machine (UTM). SEM observations revealed the presence of ferrite and austenite phases in the weld metal, heat-affected zone (HAZ), and base metal. Increased welding current, voltage, and wire feed rate promoted grain coarsening, whereas lower heat input facilitated grain refinement and enhanced grain boundary formation. The robotic pulse MIG welds exhibited a more homogeneous and refined microstructure than conventional pulse MIG welds. EDS analysis confirmed the presence of Fe-, Mn-, and Se-rich precipitates, while the concentration of secondary elements such as Si, P, and S decreased with increasing wire feed rate. Tensile testing demonstrated that robotic pulse MIG welded specimens achieved superior mechanical performance, with tensile strength ranging from 241 to 396 MPa and elongation reaching 45.1%. The optimum weld condition was obtained at 106 A current, 16.9 V voltage, 7 mm electrode stick-out, 300 mm/min welding speed, and 6.5 m/min wire feed rate, producing a tensile strength of 394 MPa. The findings indicate that robotic pulse MIG welding enhances microstructural refinement, tensile strength, ductility, and overall weld integrity, making it a reliable alternative to conventional pulse MIG welding for high-quality structural applications.

Keywords: Robotic Pulse MIG Welding, Microstructure, Tensile Properties, SEM–EDS Analysis, Heat-Affected Zone (HAZ)

INTRODUCTION

Microstructural analysis of welds is the microscopic analysis of a welded joint's internal structure to determine how the integrity and properties of the material have been affected by the welding process. By examining the microstructure, engineers can learn how the phase distribution, grain size, and appearance of any flaws like inclusions, fissures, or porosity have been affected by the welding heat and cooling rates. Three primary zones are usually examined in this process: the molten and solidified weld metal, the unaffected base metal, and the heat affected zone, which is where the base metal undergoes thermal changes without melting. These structural details are frequently revealed using methods including metallographic preparation, and scanning electron microscopy (SEM). In sectors including aerospace, automotive, and construction,

***Author for Correspondence**
Vivekanand
E-mail: var.som2020@gmail.com

[1,2]Research Scholar, Mechanical Engineering department, Faridabad College of Engineering and Management, Haryana, India

Received Date: June 16, 2026
Accepted Date: June 23, 2026
Published Date: July 14, 2026

Citation: Vivekanand and Raja Somadder. Experimental Study on Microstructural Evolution and Tensile Properties of Robotic Pulse MIG Welded Steel. Journal of Experimental & Applied Mechanics. 2026; 17(2): 40–52p.

microstructural insights are crucial for assessing mechanical attributes like strength and toughness, guaranteeing weld quality, resolving faults, and streamlining welding processes.

Microstructural analysis plays a vital role in pulse MIG welding of steel, as it provides detailed insights into the effects of input variables on the internal structure and mechanical properties of the weldment. Pulse MIG welding, which uses controlled current pulses to limit heat input and enhance metal transfer, generally produces a finer microstructure with smaller grains in both the weld region and the heat affected portion. The strength, resilience to cracking, and durability of the welded steel can all be enhanced by this refinement. We can see p hase changes, such the development of martensite, bainite, or ferrite, and any welding flaws that can impair performance, like porosity or microcracks, by looking at the microstructure. To get the greatest balance between low thermal distortion and weld quality, this information aids in optimizing the pulse parameters (peak current, pulse frequency, and background current). In the end, microstructural analysis makes sure that steel pulse MIG welding yields strong, superior welds appropriate for crucial applications in the shipbuilding, automotive, and structural sectors.

Tensile tests are performed on a Pulse MIG (Metal Inert Gas) weld to evaluate the weld strength. The tensile test is a mechanical examination that evaluates the strength and

flexibility of a welded junction by applying a uniaxial force to a specimen until it fails. It is among the most widely used techniques for figuring out a material's mechanical characteristics. In order to make sure that the weld satisfies design specifications and planned service conditions, tensile testing offers quantitative data on important factors including yield strength, ultimate tensile strength, and percentage elongation. The tensile test is frequently used in both production and qualification processes to evaluate the quality and dependability of welded joints because of its capacity to examine mechanical performance.

LITERATURE REVIEW

Metal Inert Gas (MIG) welding is one of the most widely used fusion welding processes in manufacturing industries due to its high deposition rate, ease of automation, and ability to produce quality welds. Pulse MIG welding has gained considerable attention because it offers improved control over heat input, reduced spatter formation, and enhanced weld quality compared to conventional MIG welding [1].

Several researchers have investigated the influence of welding parameters on weld microstructure and mechanical properties. Zhang and Feng [2] reported that welding heat input significantly affects grain refinement, phase transformation, and joint strength. Their findings indicated that optimized heat input leads to improved weld quality and mechanical performance. Similarly, Yan *et al*. [3] observed that controlled welding parameters promote finer microstructures and superior tensile properties in welded joints.

The relationship between microstructure and mechanical behavior has been extensively studied. Mirshekari *et al*. [4] found that refined grain structures contribute to improved tensile strength and ductility, while coarse grains reduce mechanical performance. Shanmugarajan *et al*. [5] reported that higher heat input increases the width of the heat-affected zone (HAZ) and promotes grain coarsening, thereby affecting the strength of welded joints.

The effect of process parameters such as welding speed, current, and shielding gas composition has also been examined. Zhang *et al*. [6] demonstrated that welding speed and heat input significantly influence weld penetration and tensile strength. Squillace *et al*. [7] concluded that optimized welding conditions improve weld morphology and mechanical characteristics while minimizing defects.

Pulse MIG welding has been recognized for its ability to achieve superior weld quality through controlled metal transfer. Kumar and Kumar [8] reported that pulse current parameters strongly influence residual stresses, microstructural evolution, and mechanical properties of steel weldments. Their review highlighted the importance of parameter optimization for achieving defect-free joints.

With the increasing demand for automation, robotic welding systems have become an important area of research. Studies have shown that robotic welding provides consistent heat input, precise torch movement, and improved repeatability compared to manual welding processes [9]. Wang [10] emphasized that advanced robotic welding systems equipped with intelligent sensing technologies enhance weld quality, productivity, and process reliability.

Mechanical characterization of welded joints through tensile testing remains a crucial method for evaluating weld quality. Turnage *et al*. [11] established that tensile behavior is strongly dependent on the microstructural features of the weld zone and heat-affected zone. Improved microstructural refinement generally results in higher tensile strength and ductility.

Recent reviews on welding technologies have highlighted that pulse MIG welding produces lower thermal distortion, refined grain structures, and improved mechanical properties compared with conventional welding methods [12]. Furthermore, robotic pulse MIG welding has been reported to produce stronger and more reliable welds due to stable arc characteristics and reduced process variability [13].

Although substantial research has been conducted on pulse MIG welding, limited studies have directly compared robotic pulse MIG welding with conventional pulse MIG welding through combined microstructural, compositional, and tensile analyses. Therefore, the present work focuses on evaluating the microstructure and tensile behavior of robotic pulse MIG welded steel joints and comparing the results with conventional pulse MIG weldments.

METHODOLOGY

The present study was conducted to investigate the microstructural characteristics and tensile behavior of steel weldments produced using robotic pulse MIG welding and conventional pulse MIG welding. The experimental work consisted of specimen preparation, welding under different process conditions, microstructural characterization, elemental analysis, tensile testing, and comparative evaluation of the obtained results.

Mild steel plates were selected as the base material for the welding experiments. Before welding, the surfaces of the plates were thoroughly cleaned to eliminate contaminants such as rust, oil, and dirt that could adversely affect weld quality. Eighteen welded specimens were fabricated, out of which nine specimens were produced using robotic pulse MIG welding and the remaining nine specimens were fabricated using conventional pulse MIG welding. The welding parameters were varied systematically, including welding current, voltage, electrode stick-out length, welding speed, wire feed rate, and shielding gas composition. Pure argon was used as the shielding gas for robotic pulse MIG welding, whereas a shielding gas mixture of 80% argon and 20% carbon dioxide was employed for conventional pulse MIG welding.

After welding, samples were extracted from the welded joints for microstructural examination. Scanning Electron Microscopy (SEM) was used to study the weld zone, heat-affected zone, and base metal. The SEM analysis was carried out using a JEOL JSM-6590LV microscope operating at an accelerating voltage of 10 kV, with magnifications ranging from 500× to 1500×. The analysis was performed to evaluate grain morphology, phase distribution, grain refinement, and the presence of welding defects.

The elemental composition of the weld regions was determined using Energy Dispersive X-ray Spectroscopy (EDS) integrated with the SEM system. EDS analysis was utilized to identify the distribution of alloying elements and precipitates within the weldment and to correlate the chemical composition with the observed microstructural features.

The mechanical properties of the welded joints were evaluated through tensile testing using a computer-controlled Universal Testing Machine (UTM). Dog-bone-shaped tensile specimens were prepared by Electric Discharge Machining (EDM) in accordance with standard testing procedures. During the tensile test, a uniaxial load was applied until fracture occurred, and the load-displacement data were continuously recorded. Tensile strength, yield strength, percentage elongation, maximum load, and displacement at fracture were determined from the obtained stress-strain behavior.

Finally, the results obtained from SEM, EDS, and tensile testing were analyzed and compared for both robotic pulse MIG welding and conventional pulse MIG welding. The influence of welding parameters on microstructural evolution and mechanical performance was evaluated to determine the optimum welding conditions capable of producing superior weld quality, enhanced tensile strength, and improved ductility.

EXPERIMENTATION

Experimental Procedure

The SEM–EDS system shown in the figure 1 provides an integrated platform for detailed microstructural and compositional characterization. SEM offers high-resolution imaging necessary for analyzing grain structures, weld zones, fracture surfaces, and surface morphology, while EDS provides essential elemental information. This combined functionality makes the setup indispensable for materials science research, especially in areas such as welding metallurgy, failure analysis, surface engineering, and quality control.

Scanning Electron Microscopy

SEM creates images with great resolution by scanning the specimen's surface with an electron beam, allowing for accurate detection of microstructural details. SEM experiments were performed in Physics department, NIT Kurukshetra, Haryana India. SEM experimental setup is shown in figure 1. The SEM column, which contains the electron gun, electromagnetic lenses, scanning coils, and specimen chamber, is the main part of the apparatus. A concentrated beam of high-energy electrons is employed by the SEM to scan the specimen's surface in a raster pattern. When the electron beam strike on the target, it produces signals such as secondary electrons, backscattered electrons, and characteristic X-rays. Detectors gather these signals to create high-resolution pictures with superior depth of field. The SEM seen in the picture (JEOL JSM-6590LV) can analyze both conductive and non-conductive materials since it can function in both high-vacuum and low-vacuum modes. Microstructural analysis was performed on small specimen of size 10 mm x10 mm x 4 mm. Microstructure of the weldment was analysed at different SEM input parameters. SEM experiments were performed at accelerating voltage 10 kV, working distance 10 µm to 50 µm and magnification 500x to 1500x.

Energy Dispersive X-ray Spectroscopy (EDS)

The EDS detector is a crucial component for compositional analysis and is installed at an angle to the SEM chamber. Characteristic X-rays are released when the specimen's atoms contact with the main electron stream. In order to identify the elements contained in the material and determine their relative concentrations, the EDS detector monitors the energy and intensity of these X-rays. Correlation between microstructure and chemistry is made possible by the simultaneous imaging and elemental mapping made possible by the integration of the EDS detector with the SEM. The X-ray spectra obtained from the specimen may be acquired and interpreted thanks to the EDS gear and related software. The system offers elemental mapping, peak recognition, quantitative analysis, and real-time spectrum visualization. For the analysis of inclusions, precipitates, weld interfaces, diffusion zones, and microstructural heterogeneities, this capacity is very useful.

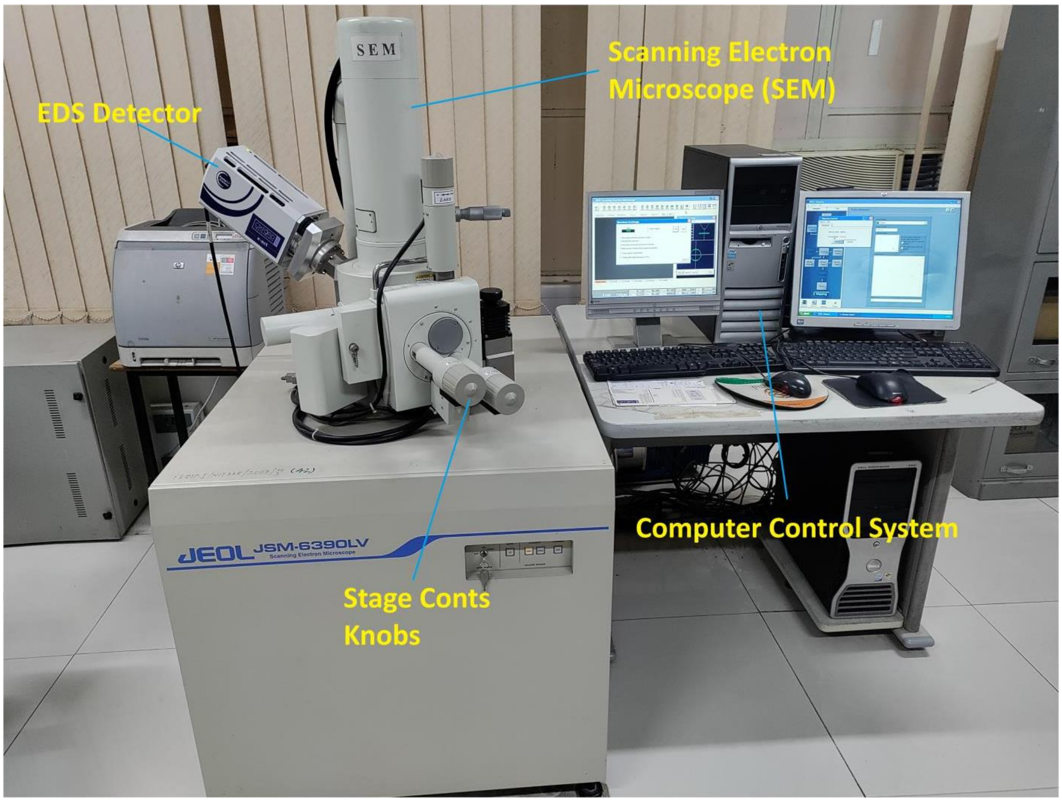

Figure 1. SEM-EDS experimental setup

Tensile Test using Universal Testing Machine (UTM)

The computer controlled mechanical universal testing machine is utilized for testing weldment mechanical properties such as tensile strength, elongation, yield strength and ultimate tensile strength. The experimental setup of universal testing machine is shown in figure 2. The figure shows a complete tensile testing setup consisting of an FIE Universal Testing Machine (UTM) and its computer-based data acquisition system. The UTM uses a sturdy vertical frame, a moveable crosshead, and specially made grips to provide a controlled uniaxial tensile force to the specimen while it is being tested. The specimen elongates till failure as the upper crosshead rises, and the integrated load cell continually monitors the applied stress. The computer interface used to track and record the tensile test in real time. The load-displacement curve, which shows the material's elastic area, yielding, plastic deformation, strain hardening, and ultimate fracture, is automatically shown by the program. Additionally, the interface shows computed mechanical parameters including tensile strength, elongation, yield load, and maximum load. This configuration is crucial for evaluating the performance of materials in welding and structural applications as it guarantees precise and trustworthy assessment of the mechanical behavior of welded and base metal specimens.

The electric discharge machining (EDM) technique was used to cut eighteen dog bone-form test pieces from the welded plate along the transverse direction of the weld. Figure 3 show the tensile test specimen of sample L1 to L9.

RESULTS AND DISCUSSIONS

Variations in pulse MIG welding settings cause discernible changes in the microstructure of both the weld zone and the heat-affected zone (HAZ), according to microstructural examination using SEM. SEM pictures show that the weldment contains both austenite and ferrite phases. Furthermore, greater grain sizes were found to be produced by higher welding voltages, as seen in Figure 4. Because of the impact of heat cycles on microstructural development, the grains in the HAZ were coarser than those in the base metal and weld zone. The formation of pearlite structure decrease as current and voltage increase. The grain size grew as the wire feed rate increased. Lower temperatures and voltage contribute to the nucleation of edges and the development of grain boundaries.

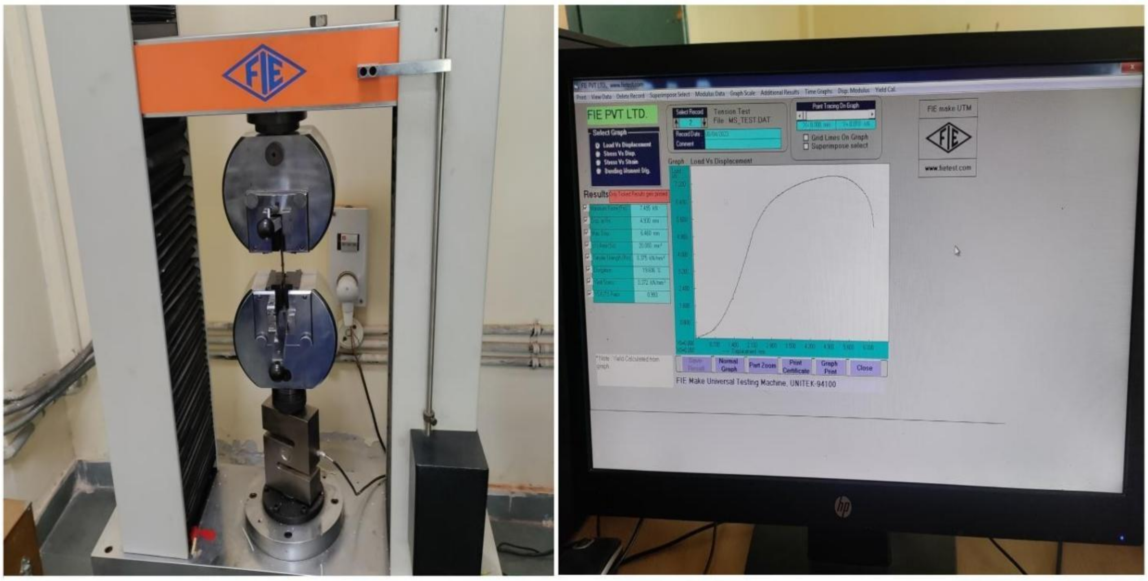

Figure 2. Computer Controlled Universal Testing Machine

Figure 3. Robotic pulse MIG welding Specimens for tensile test

The experimental results reveal that, at an unchanged welding current is the same, the remaining welding input parameters have relatively little influence on the microstructure of the HAZ when compared to the weld zone (WZ). The microstructure of both the HAZ and WZ was found to be more uniform and finer in the case of the weld specimen obtained using robotic pulse MIG welding as compared to conventional pulse MIG welding as presented in Fig 5 (a) and (b), respectively. The best results were obtained using the following parameters: moderate current (106 A), voltage (16.9 V), electrode stick-out length (7 mm), welding speed (300 mm/min), and wire feed rate (6.5 m/min).

The elemental percentage fluctuation in different weld zones was determined using SEM in combination with EDS analysis. The SEM images with EDS results are given in Figure 4.6.

According to Figure 6, the EDS test revealed the existence of Se, Mn, and Fe-rich precipitates in welds A and B, respectively. The size of the precipitates differed from each other but did not change significantly in response to heat input. It has been observed that the presence of secondary micro-constituents Si, P, and S reduced when wire feed rate is increased.

The tensile properties of all the samples S1-S18 are determined using Table 1 and summarized in Table 2. Table 2 presents the output responses (maximum load, maximum displacement, tensile strengths, elongation, and yield strengths) of each sample with respect to the various input factors of Table 1 (shielding gas, average current/voltage, electrode stickout length, welding speed, and wire feed rate). As indicated in Tables 1 and 2, the first nine samples (S1-S9) were made using robotic pulse MIG welding, whereas the next nine samples (S10-S18) were fabricated using the basic pulse welding method.

A collection of tensile test specimens both before and after testing is seen in figure 7. The prepared dogbone-shaped specimens in their original, undisturbed state are shown in the top row. These samples have a uniform gauge section in the center where deformation is anticipated, and they have been machined to typical tensile dimensions. The obvious weld bead or heat-affected zone in the middle of the specimens suggests that they are welded samples. During tensile testing, their homogenous shape guarantees constant loading.

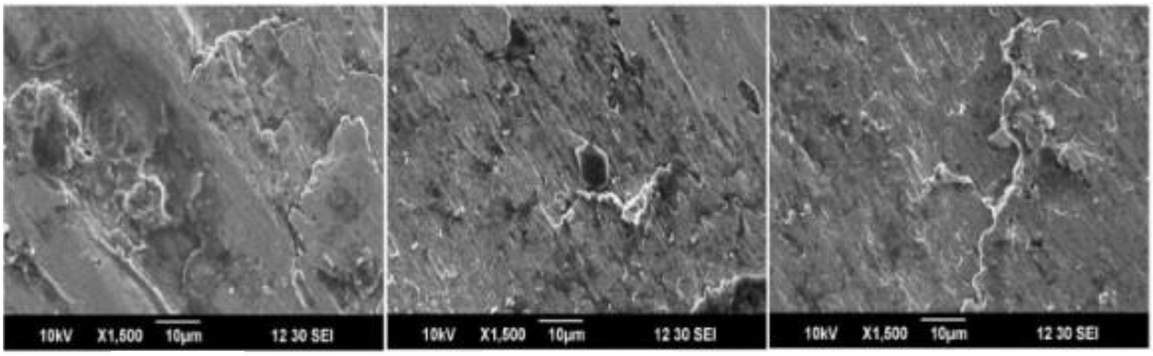

Base Material Heat Affected Zone Weld Zone

Figure 4. Microstructure of weld specimen

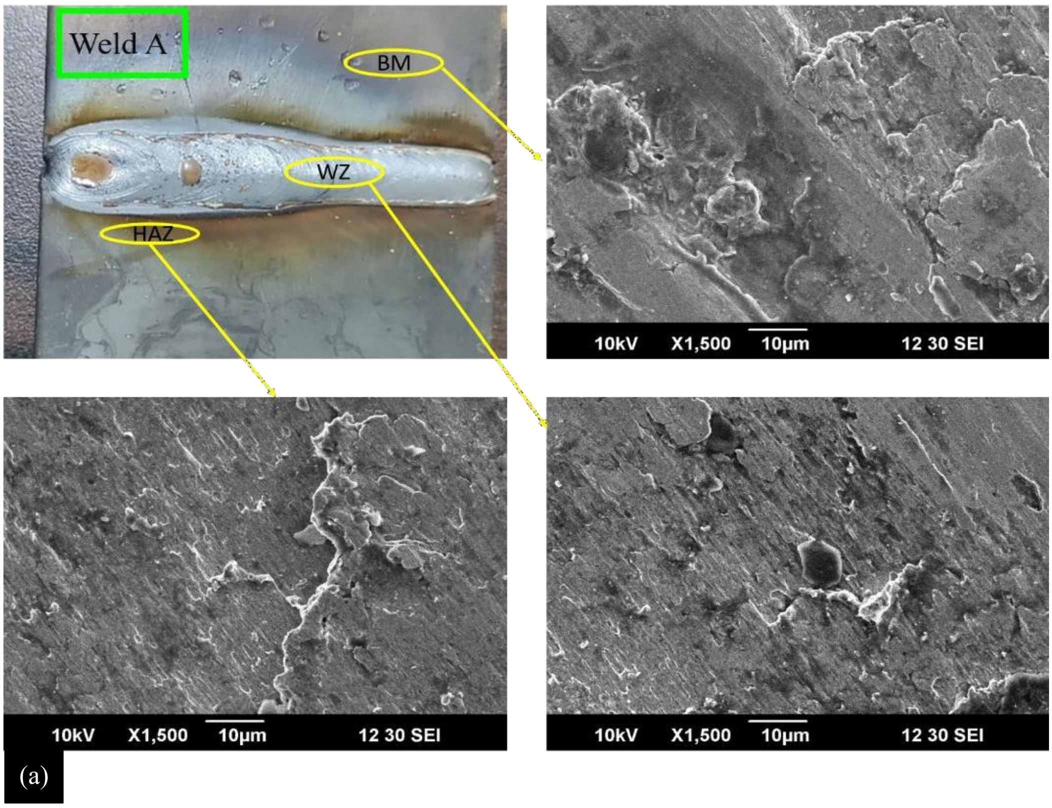

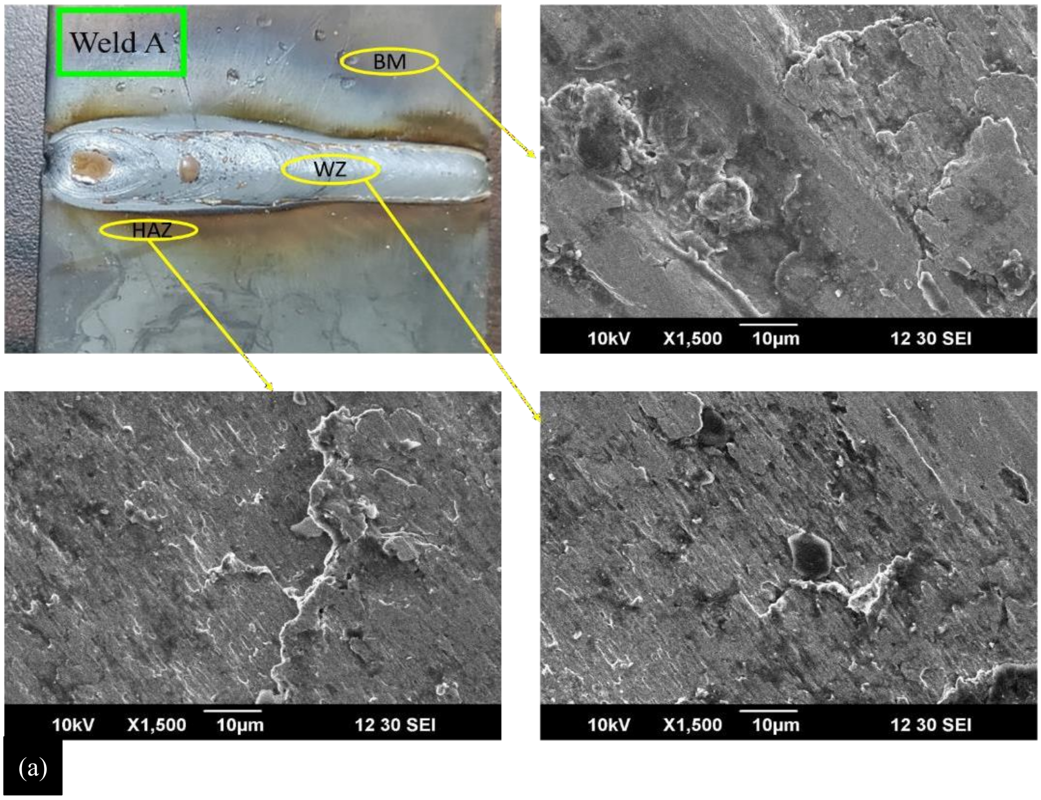

Figure 5. Microstructural characterization (a) SEM photographs of a weld manufactured by general pulse MIG technique (b) SEM photographs of specimen manufactured using robotic pulse MIG technique

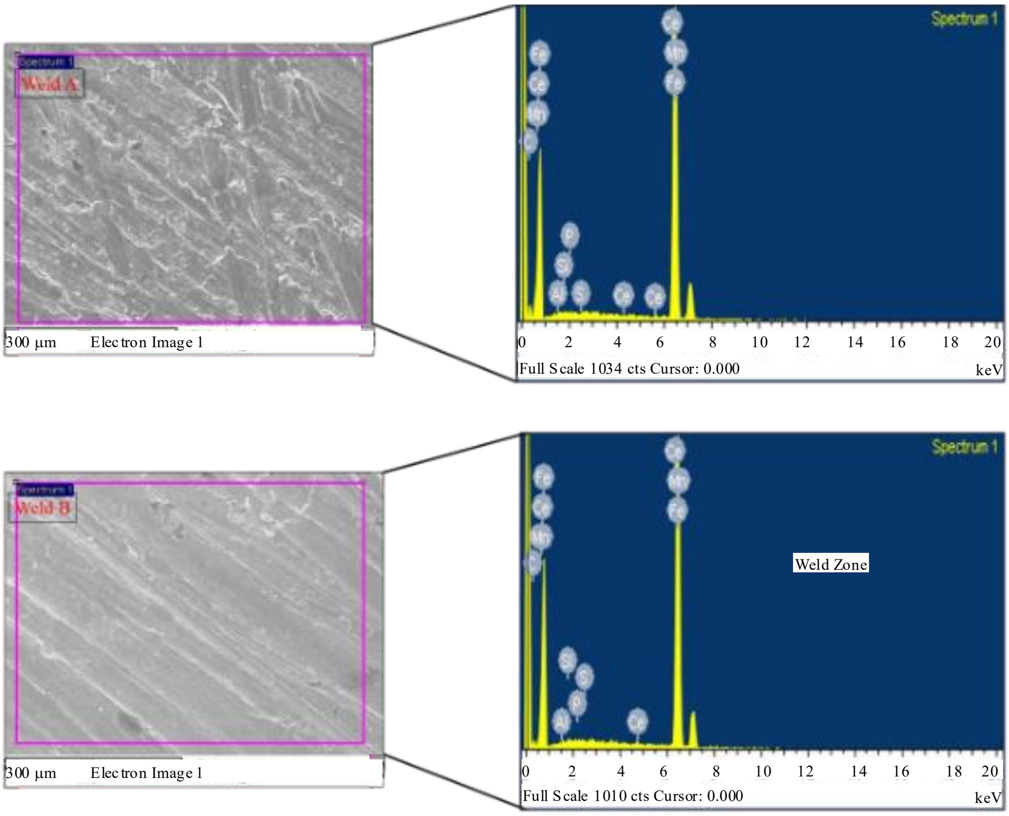

Figure 6. Evaluation of chemical composition of the weld samples using EDS technique

Figure 7. Fracture samples of tensile test

The same specimens following tensile testing are displayed in the bottom row. The gauge sections clearly show necking and fracture, revealing the areas with the highest concentrations of tensile stress. While some specimens appear to have cracked close to the weld joint, indicating reduced strength in those particular samples, the majority show ductile failure which is characterized by regional thinning and extended fracture surfaces. Differences in the specimens' tensile characteristics, microstructural alterations, or weld quality are highlighted by the variances in fracture position and deformation behavior. This visual comparison of pre-test and post-test samples shows how the welded material responds mechanically to uniaxial tensile loads and sheds light on the integrity and performance of the weld.

The tensile strengths of the test parts welded by robotic pulse MIG welding vary between 241 and 394 MPa. In a similar vein, test samples fused using a simple pulse welding approach demonstrated tensile values ranging from 9 to 382 MPa. The peak value of tensile strength for the weldment was seen in the case of sample 2 at the optimal input parameters of 100% argon as shielding gas, 106 A current/16.9 V voltage, 7 mm electrode stick-out length, welding speed of 300 mm/min, and wire feed rate 6.5 m/min, respectively. The maximum elongation of the test pieces for robotic MIG is between 13.4 and 45.1%, whereas it is between 4.2 and 42.8% for pulse MIG weldments.

Table 1. Input parameters to fabricate different weld samples

Sample No.	Shielding Gas mixture (%)	Welding current (A)/ voltage (V)		Electrode stick-out length (mm)	Welding Torch speed (mm/min)	Wire feed rate (m/min)
Test samples fabricated using robotic pulse MIG welding						
1	Argon	62	15.7	4	200	4
2	Argon	106	16.9	7	300	6.5
3	Argon	134	18.1	10	400	9
4	Argon	106	16.9	4	300	6.5
5	Argon	134	18.1	7	400	9
6	Argon	62	15.7	10	200	4

Sample No.	Shielding Gas mixture (%)	Welding current (A)/ voltage (V)		Electrode stick-out length (mm)	Welding Torch speed (mm/min)	Wire feed rate (m/min)
7	Argon	134	18.1	7	200	9
8	Argon	62	15.7	10	300	4
9	Argon	106	16.9	4	400	6.5
Test samples fabricated using conventional pulse MIG welding						
10	Ar= 80 CO_2 = 20	106	16.9	10	400	6.5
11	Ar= 80 CO_2 =20	134	18.1	4	200	9
12	Ar= 80CO_2 = 20	62	15.7	7	300	4
13	Ar= 80 CO_2 = 20	62	15.7	7	400	4
14	Ar= 80 CO_2 = 20	106	16.9	10	200	6.5
15	Ar= 80 CO_2 = 20	134	18.1	4	300	9
16	Ar= 80 CO_2 = 20	134	18.1	10	300	9
17	Ar= 80 CO_2 = 20	62	15.7	4	400	4
18	Ar= 80 CO_2 = 20	106	16.9	7	200	6.5

Table 2. Tensile test output responses of different welding samples

Sr. No.	Maximum load, kN	Maximum displacement, mm	Tensile strength, MPa	Maximum elongation, %	Yield strength, MPa
1	7.50	6.4	375	19.6	372
2	9.45	9.0	394	36.1	343
3	9.01	10.6	376	42.5	371
4	7.81	5.0	326	20.2	321
5	9.00	9.9	379	39.7	374
6	5.93	4.3	247	17.2	247
7	9.51	11.3	396	45.1	335
8	5.77	3.3	241	13.4	241
9	8.96	11.1	374	44.4	366
10	0.31	2.1	78.0	22.2	77.0
11	1.02	2.0	11.0	20.2	14.0
12	6.40	7.7	211	35.2	211
13	0.21	2.6	9.00	10.5	9.00
14	0.82	1.0	34.0	4.2	34.0
15	9.09	10.6	379	42.7	355
16	9.08	10.7	379	42.8	349
17	9.17	10.1	382	40.4	354
18	0.20	2.1	9.50	9.42	9.54

Figure 8 shows the load versus displacement plots of the samples (S2, S8, S17, and S13) with the highest and lowest tensile strengths. The load versus displacement curves show that the displacements of the curve at maximum loads (9.45 KN and 5.77 KN) are 6.5 mm and 3.2 mm, respectively, when the samples are joined together using the Robotic MIG welding process. Similarly, samples welded using pulse MIG welding have curve displacements of 7.27 and 0.310 mm at maximum loads of 9.17 KN and 0.21 KN, respectively. It can be determined that weldments formed utilizing the robotic MIG welding technology have higher strength values (tensile, yield, and upper yield) at maximum load and are similar to the standard stress–strain curve of mild steel.

Journal of Experimental & Applied Mechanics
Volume 17, Issue 2
ISSN: 2230-9845 (Online), ISSN: 2321-516X (Print)

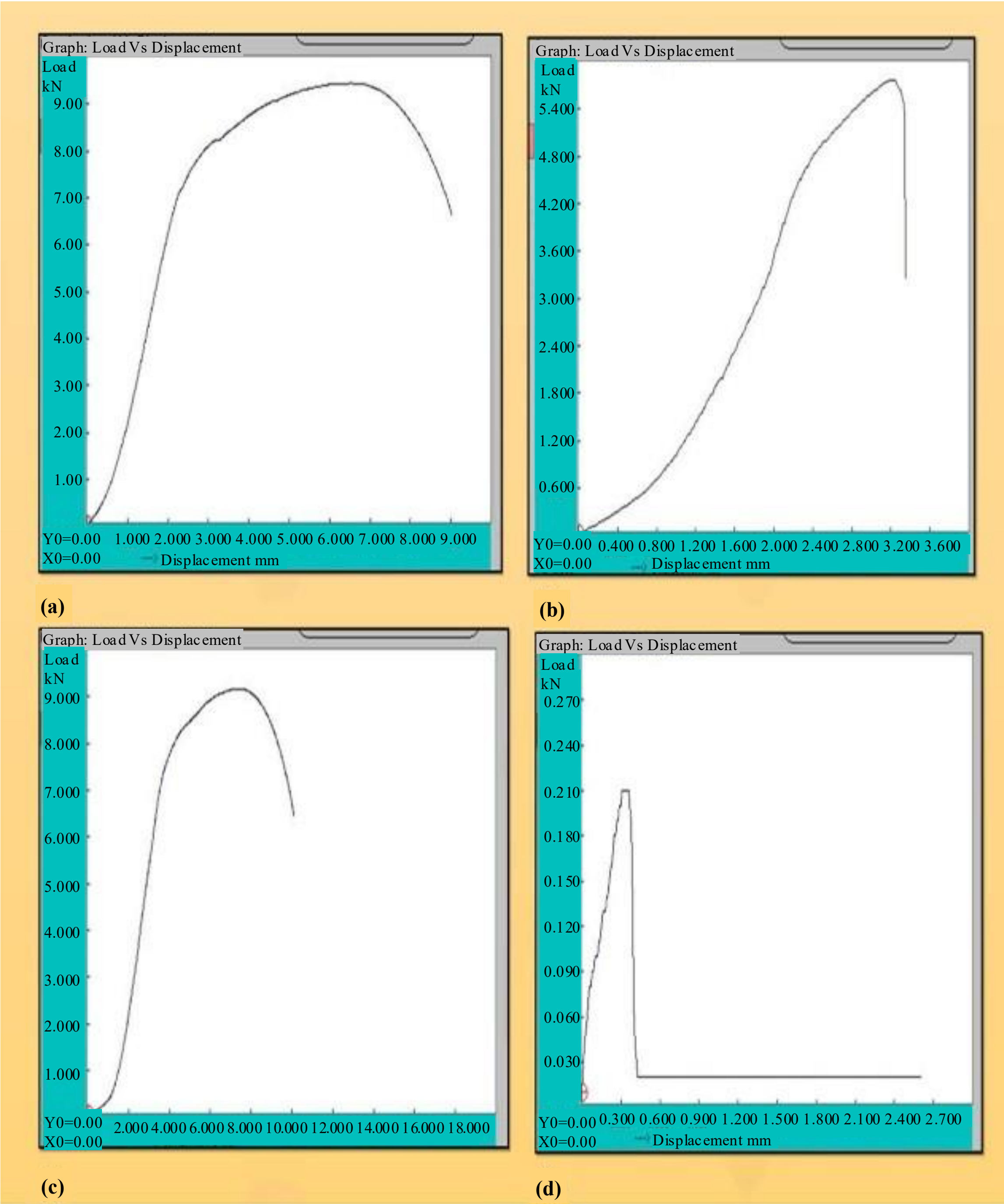

Figure 8. Load versus displacement curves of weldment test pieces

Figure 9 and 10 illustrates fluctuations in the maximum tensile and yield strength values of test pieces generated by robotic and pulse MIG welding. The following three figures illustrate that specimens welded using the robotic pulse MIG welding technology have higher strengths and mechanical qualities. The specimens joined using simple MIG welding have poor weld characteristics in terms of mechanical properties and strengths.

When compared to traditional MIG, the robotic MIG welded samples exhibit higher mechanical performance, as evidenced by the load-displacement curves obtained from tensile testing. Because of steady arc control and constant heat input, robotic welders have a steeper initial slope, which indicates greater stiffness and more consistent elastic behavior. Robotic specimens had a much higher peak load, indicating that these joints can sustain larger tensile stresses before failing. Furthermore, robotic welds often exhibit a greater displacement during fracture, indicating enhanced energy absorption and ductility. Their curves exhibit a more gradual post-peak decline and increase gradually to the maximum load, suggesting steady fracture propagation and fewer internal flaws. On other hand, Because of operator-dependent inconsistencies such unequal heat input, varied penetration, and a larger chance of flaws, traditional MIG welded joints exhibit increased variability, lower maximum loads, and decreased fracture displacement. Conventional welds frequently show non-uniform behavior in their load-displacement response, with early yielding or abrupt dips that may indicate stress concentration zones or microcracks inside the weld zone. In comparison to manual conventional MIG welding, robotic MIG welding generally results in stronger, more ductile, and more dependable welds, according to tensile test findings.

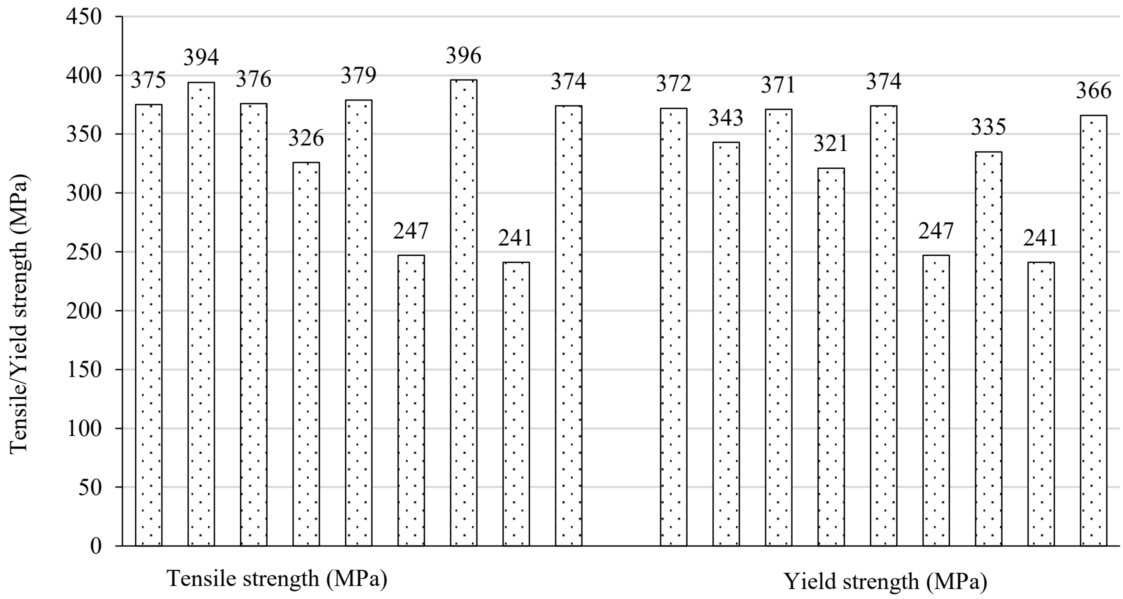

Figure 9. Tensile/yield strengths of test specimen welded by Robotic pulse welding process

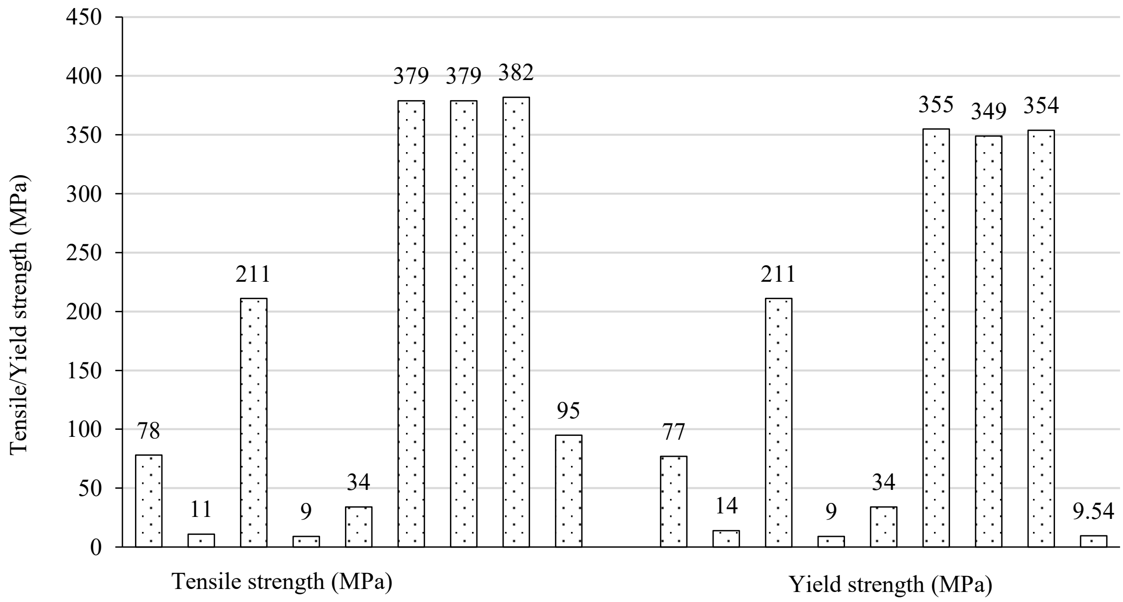

Figure 10. Tensile/yield strengths of test specimen welded by pulse welding process

CONCLUSION

In conclusion, this chapter investigated the microstructure and tensile behaviour of the MIG welded joints to understand the relationship between weld metallurgy and mechanical performance. Due to variances in input parameters during pulse MIG welding, the microstructural analysis showed notable discrepancies in grain structure and phase distribution throughout the base metal, heat impacted zone, and weld zone. The tensile characteristics of the welded connections were significantly influenced by these microstructural differences. The findings of tensile tests showed that the properties of the weld metal and heat-affected zone had a significant impact on joint strength and ductility. The impact of microstructural variation on tensile performance was further supported by the observed fracture behavior. Overall, the results show that better microstructural refinement and improved tensile behavior result from optimized welding conditions, which helps to create dependable and high-quality welded connections.

REFERENCES

1. K. Weman, *MIG Welding Guide*, Cambridge, U.K.: Woodhead Publishing, 2012.
2. H. T. Zhang and J. C. Feng, “Microstructure and properties of aluminum-zinc coated steel lap joints fabricated by modified MIG weld brazing process,” *Materials Characterization*, vol. 58, no. 7, pp. 588–592, 2007.
3. S. Yan, C. Ge, Z. Lin, and W. Shan, “Mechanical properties and microstructure of hybrid laser-MIG welded AA6005-T5 alloy,” *Materials Science and Engineering A*, vol. 559, pp. 229–235, 2013.
4. G. R. Mirshekari, A. Saatchi, A. Kermanpur, and S. K. Sadrnezhaad, “Effect of welding parameters on microstructure and mechanical properties of welded joints,” *Optics & Laser Technology*, vol. 54, pp. 151–158, 2013.
5. B. Shanmugarajan *et al*., “Studies on autogenous laser welding of stainless steel,” *Optics and Lasers in Engineering*, vol. 51, no. 12, pp. 1272–1277, 2013.
6. M. Zhang, G. Chen, Y. Zhou, and S. Liao, “Optimization of deep penetration welding parameters for stainless steel,” *Materials and Design*, vol. 53, pp. 568–576, 2014.
7. A. Squillace, U. Prisco, S. Ciliberto, and A. Astarita, “Effect of welding parameters on morphology and mechanical properties of welded joints,” *Journal of Materials Processing Technology*, vol. 212, no. 2, pp. 427–436, 2012.
8. S. Kumar and V. Kumar, “Residual stress analysis during pulse MIG welding of steel: A review,” *International Journal of Engineering Research*, vol. 8, no. 4, pp. 112–118, 2020.
9. S. K. Singh, R. Kumar, and P. Sharma, “Investigation of microstructure and mechanical properties of robotic MIG welded steel joints,” *International Journal of Mechanical Engineering*, vol. 12, no. 12, pp. 1–12, 2025.
10. Z. Wang, “The active visual sensing methods for robotic welding: Review, tutorial and prospect,” *IEEE Access*, vol. 12, pp. 45621–45645, 2024.
11. S. A. Turnage *et al*., “Quantifying structure–property relationships during resistance spot welding,” *Materials Characterization*, vol. 112, pp. 10–19, 2016.
12. A. G. Olabi *et al*., “A review on welding techniques: properties, processes and applications,” *Welding International*, vol. 37, no. 3, pp. 145–168, 2023.
13. J. Norrish, *Advanced Welding Processes*, 2nd ed. Cambridge, U.K.: Woodhead Publishing, 2017.

